JOURNAL OF GEOPHYSICAL RESEARCH, VOL. 91, NO. A9, PAGES 10,013–10,028, SEPTEMBER 1, 1986

Waves and Electric Fields Associated With the First AMPTE Artificial Comet

D. A. GURNETT,[1] R. R. ANDERSON,[1] T. Z. MA,[1] G. HAERENDEL,[2] G. PASCHMANN,[2] O. H. BAUER,[2] R. A. TREUMANN,[2] H. C. KOONS,[3] R. H. HOLZWORTH,[4] AND H. LÜHR[5]

A variety of plasma wave and electric field effects were observed during the AMPTE (Active Magnetospheric Particle Tracer Explorers) solar wind barium release on December 27, 1984. Electron plasma oscillations provided measurements of the electron density during the entire event. Inside the diamagnetic cavity created by the ion cloud, the electron density reached a peak of about 2×10^5 cm^{-3} and then decreased approximately as t^{-2} as the cloud expanded. A static electric field of about 1–2 mV/m was detected in the diamagnetic cavity. This electric field is in the same direction as the solar wind electric field, suggesting that the solar wind electric field may be able to penetrate into the cloud. As the spacecraft passed through the boundary of the diamagnetic cavity, a region of compressed plasma and magnetic field was detected upstream of the ion cloud with a peak density of about 10^4 cm^{-3} and magnetic field strength of 130 nT. This region of compressed plasma is believed to be caused by solar wind plasma and magnetic field lines draped around the nose of the ion cloud. Inside the diamagnetic cavity, electrostatic emissions were observed in a narrow band centered on the barium ion plasma frequency and in another band at lower frequencies. These waves are believed to be short-wavelength ion acoustic waves. Bursts of electrostatic waves were also observed at the boundaries of the diamagnetic cavity, apparently caused by an electron drift current along the boundary. An intense burst of broadband electrostatic noise was observed near the outer boundary of the plasma compression region with intensities of up to 140 mV/m. This noise is apparently associated with a shocklike interaction between the ion cloud and the solar wind. Growth rate computations show that the noise can be accounted for by an electrostatic ion beam-plasma interaction between the nearly stationary barium ions and the rapidly moving solar wind protons.

1. INTRODUCTION

The first attempt to produce a man-made comet was performed on December 27, 1984, as part of the AMPTE (Active Magnetospheric Particle Tracer Explorers) program. The primary objective of the AMPTE program was to use barium and lithium ions as tracers to study the transport and energization of charged particles in the earth's magnetosphere [*Krimigis et al.*, 1982]. A secondary objective was to simulate the solar wind–plasma interactions of a natural comet by releasing a cloud of barium gas in the solar wind. The possibility of simulating a comet by artificial gas releases in the upper atmosphere was first suggested by *Biermann et al.* [1961]. Since the original suggestion by Biermann et al., various techniques have been developed to produce artificial gas releases by using explosive charges carried aloft by rockets. For a review of the techniques used over the past 20 years, see *Pongratz* [1981]. In most cases the material used for the gas release has been either barium, cesium, or lithium. The choice of material is determined by the desire to have a short ionization time and optical scattering properties suitable for ground-based optical observations. Barium releases have been used as tracers to determine plasma convection velocities in the ionosphere [*Haerendel et al.*, 1967; *Föppl et al.*, 1968; *Haerendel and Lüst*, 1968; *Wescott et al.*, 1969; *Heppner et al.*, 1971] and in the magnetosphere [*Mende*, 1973; *Adamson et al.*, 1973]. Special shaped charge releases have been used to probe for parallel electric fields in the auroral zone and polar cap [*Haerendel et al.*, 1976; *Wescott et al.*, 1980]. Barium and cesium releases have also been employed to trigger waves and instabilities in the ionosphere [*Koons and Pongratz*, 1979; *Kintner et al.*, 1980].

Although numerous artificial gas releases have been performed in the ionosphere and magnetosphere, the first true artificial comet experiment, intended to simulate the interaction with the solar wind, was carried out by the AMPTE project. Two artificial comet releases were performed: the first on December 27, 1984, and the second on July 18, 1985. The purpose of this paper is to provide a detailed discussion and analysis of the plasma wave observations obtained during the first release on December 27, 1984. The second release will be discussed in a future paper.

The AMPTE project consists of three spacecraft: the Ion Release Module (IRM), which carried the barium and lithium canisters; the United Kingdom Satellite (UKS), which flew near the IRM to study the expansion and evolution of the ion cloud; and the Charge Composition Explorer (CCE), which was designed to detect the tracer ions in the inner regions of the magnetosphere. The data presented in this paper are from the IRM. The IRM is in a low-inclination, highly eccentric orbit with an apogee geocentric radial distance of about 19 R_E. The barium cloud was produced by releasing two canisters containing barium in diametrically opposite directions from the IRM. Ten minutes after the release the two canisters were exploded simultaneously at a distance of about 1 km from the spacecraft. The explosions produced a rapidly expanding cloud of neutral barium which swept over the spacecraft a fraction of a second later. As the cloud expanded, ultraviolet radiation from the sun ionized the gas, forming a dense cloud of ionized barium. For barium the ionization time constant is

[1] Department of Physics and Astronomy, University of Iowa, Iowa City.
[2] Max-Planck-Institut für extraterrestrische Physik, Garching, Federal Republic of Germany.
[3] The Aerospace Corporation, Los Angeles, California.
[4] Geophysics Program, University of Washington, Seattle.
[5] Institut für Geophysik und Meteorologie, Technische Universität Braunschweig, Braunschweig, Federal Republic of Germany.

Paper number 5A8338.
0148-0227/86/005A-8338$05.00

quite short, only about 28 s [*Carlsten*, 1975], so most of the ionization occurs within the first minute. For a discussion of the physics of the cloud formation and expansion, see *Haerendel* [1983].

A wide variety of particle and field instruments were used on the IRM to analyze plasma effects produced by the ion cloud. A list of all the instruments on the spacecraft is given by *Krimigis et al.* [1982]. The measurements of particular interest for this study are from the plasma wave instrument, the plasma instrument, and the magnetometer. The plasma wave instrument uses a 47-m tip-to-tip electric dipole antenna for electric field measurements and two search coil magnetometers for magnetic field measurements. The signals from these antennas are processed by a variety of receivers and analyzers provided by three groups: the University of Iowa, the Max-Planch-Institut, and the Aerospace Corporation. This combined instrumentation provides spectrum measurements from 0 to 6 MHz for the electric field, and from 30 Hz to 2 MHz for the magnetic field. For a description of the plasma wave instrument, see *Häusler et al.* [1985]. The plasma instrument on the IRM provides full three-dimensional measurements of the electron and ion distribution functions once every spacecraft rotation (~4.4 s). The energy range is 15 eV/q to 30 keV/q for electrons and 20 eV/q to 40 keV/q for ions. For a description of the plasma instrument, see *Paschmann et al.* [1985]. The magnetic field instrument on the IRM is a three-axis magnetometer with a dynamic range of 0.1 to 60,000 nT. For a description of the magnetometer, see *Lühr et al.* [1985].

The first AMPTE artificial comet experiment was performed on December 27, 1984. The canisters were released at 1222:00 UT and exploded at 1232:00 UT. The distance between the canisters and the spacecraft at the time of the explosion is estimated to be 0.87 km. The IRM at this time was in the solar wind on the morningside of the earth at a geocentric radial distance of 17.2 R_E and a local time of 0706 hours. The barium ion cloud produced by the explosion was observed on the ground for a period of several minutes. For an initial report on the optical, plasma, magnetic field, and plasma wave effects observed during this release, see the series of papers by *Haerendel et al.* [1986], *Valenzuela et al.* [1986], *Rees et al.* [1986], *Lühr et al.* [1986], *Rodgers et al.* [1986], and *Gurnett et al.* [1985].

2. Plasma Density

One of the primary objectives of the plasma wave investigation on the IRM was to measure the electron density of the plasma cloud produced by the explosion. Two effects provided information on the electron density. The first effect is the presence of electrostatic oscillations at the electron plasma frequency. These oscillations can be seen in the spectrogram of Plate 1 starting shortly after the explosion at 1232:00 and extending to about 1234:20. The narrow-band character of the emissions and their similarity to previous spacecraft observations [*Scarf et al.*, 1971] uniquely identify these waves as electron plasma oscillations. Because the oscillations are at the local electron plasma frequency, which is given by $f_p = 9000\ (N_e)^{1/2}$ Hz, where N_e is the electron number density in cm^{-3}, a measurement of the emission frequency gives the local electron density. The second effect is the presence of a propagation cutoff in the galactic and terrestrial radio emissions. This propagation cutoff can be clearly seen in Plate 1 at a frequency of about 2 or 3 times the local electron plasma frequency. The cutoff is caused by the high electron density in the cloud, which blocks all external radiation at frequencies below the electron plasma frequency. As is well known [*Krall and Trivelpiece*, 1973], free space electromagnetic radiation cannot propagate at frequencies below the electron plasma frequency.

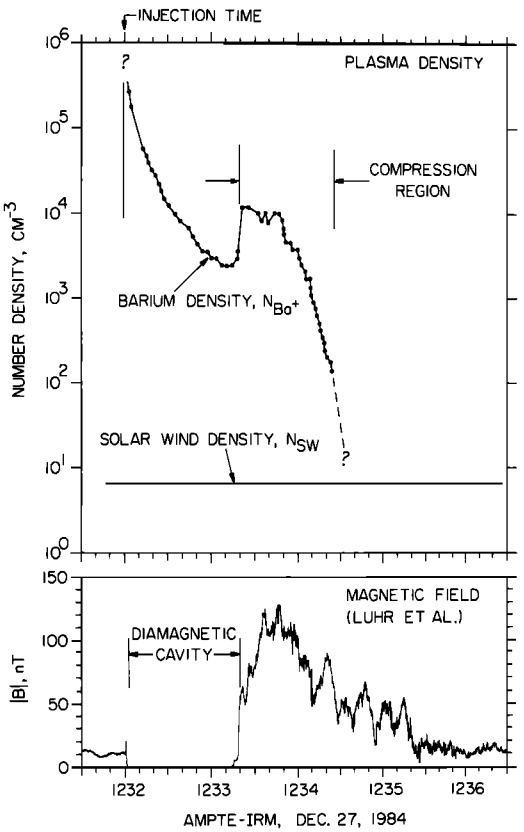

Fig. 1. The top panel shows the electron number density as obtained from the electron plasma oscillation line in Plate 1. The bottom panel shows the magnetic field |**B**| from the magnetometer. Two distinct regions can be identified: the diamagnetic cavity where |**B**| = 0, and the plasma compression region where the plasma density and magnetic fields are temporarily enhanced by the interaction with the solar wind.

The top panel of Figure 1 shows the electron density variation obtained from the electron plasma oscillations. Each point represents a single sweep of the spectrum analyzer. As can be seen, within a fraction of a second after the explosion, the electron density jumps nearly 5 orders of magnitude, up to about 2×10^5 cm^{-3}, and then decays back to the ambient solar wind density over a period of about 2 min. For a few brief periods, particularly early in the event, the plasma oscillations were too weak to provide reliable measurements. The density profile is interpolated through these regions by straight lines. After about 1234:25 the electron plasma oscillations become very difficult to identify. Other less well-resolved emissions at lower frequencies suggest that the electron density continues to decline steeply, as indicated by the dashed line. The solid horizontal line shows the nominal solar wind density before the event. Barium ions are believed to constitute the dominant component of the cloud from 1232:00 to at least 1234:25, after which the solar wind protons are dominant. Since the barium ions are singly charged and the plasma is electrically neutral, the barium ion density in the central region of the cloud is approximately equal to the electron density, $N_{Ba^+} = N_e$.

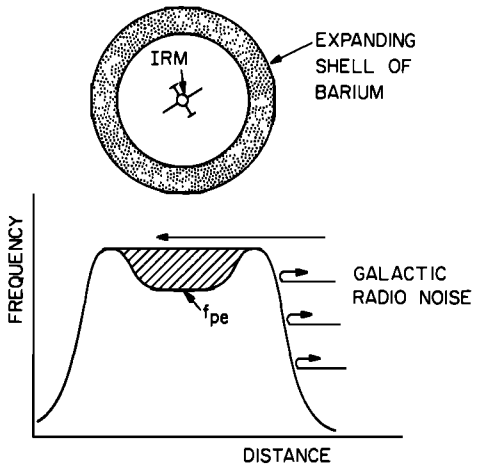

Fig. 2. The fact that the galactic radio noise cutoff is above the local electron plasma frequency suggests that the ion cloud is initially expanding as a dense shell with a depleted inner core. The depletion produces a gap (hatched) between the galactic cutoff and the local plasma frequency f_{pe}.

The density variations at the IRM are controlled by two processes, expansion and convection. During the expansion phase, which extends up to about 1233, the density decreases monotonically as the cloud expands radially outward. The expansion phase continues until about 1233:15, with the density varying approximately as t^{-2}. During the expansion phase the spacecraft is in a region of essentially zero magnetic field created by the expanding, highly conducting ion cloud. For comparison the magnetic field is shown in the bottom panel of Figure 1. The region of zero field is called the diamagnetic cavity. For a further discussion of the diamagnetic cavity, see *Lühr et al.* [1986].

Information on the structure of the expanding ion cloud can be obtained from the propagation cutoff of the galactic radio noise. Early in the expansion phase the cutoff of the galactic radio noise is at a frequency of about 2 or 3 times the local electron plasma frequency. Our interpretation of the gap between the propagation cutoff and the local electron plasma frequency is that the ion cloud consists of a dense expanding shell with a depleted inner core, such as is illustrated in Figure 2. Because the galactic radio noise is blocked by the expanding shell, the frequencies indicated by hatching are not accessible to the incoming radiation. This explains why the propagation cutoff observed by the IRM in the center of the cloud is above the local electron plasma frequency. The observed cutoffs suggest that the plasma density at the center of the cloud may be much as a factor of 10 lower than the density in the expanding spherical shell.

The first evidence of a deviation from simple radial expansion is at 1233-15, where the density suddenly increases up to about 10^4 cm^{-3}. As can be seen from the bottom panel of Figure 1, this increase coincides almost exactly with the return of a strong magnetic field, much stronger than the field that existed before the event. The interpretation of these effects is that the cloud has started to convect, thereby causing the spacecraft to enter a region of compressed plasma upstream of the ion cloud. The magnetic field lines in this region are draped around the nose of the cloud as shown in Figure 3. Although the cloud must eventually be carried downsteam by the solar wind, ground optical observations [*Rees et al.*, 1986] show that the initial motion is actually perpendicular to the solar wind flow. The approximate trajectory of the IRM relative to the diamagnetic cavity is shown by the dashed line in Figure 3. The motion perpendicular to the solar wind flow is believed to be a reaction to the acceleration of barium ions away from the cloud by the solar wind electric field. For a discussion of the cloud dynamics, see *Haerendel et al.* [1986]. Optical observations [*Rees et al.*, 1986] indicate that the diamagnetic cavity expanded to a maximum radius of about 100 km about 2–3 min after the explosion. After this time the cloud was rapidly swept downstream by the solar wind.

3. Static Electric Field

In addition to wave measurements the plasma wave instrument also provides measurements of the static electric field. The static electric field measurements obtained during the artificial comet experiment are shown in Figure 4. The top panel shows the E_x component of the electric field as detected in the low-frequency waveform channel. This channel has a passband from 0.1 to 20 Hz. A nearly sinusoidal spin modulation signal, indicative of a static electric field, is clearly evident after 1232:00. Before the explosion, prior to 1232:00, a very strong spin modulation signal is present that saturates the waveform channel. This signal is caused by the photoelectron cloud from the spacecraft. Because the electric antenna is relatively short, only 47.4 m tip to tip, the spacecraft photoelectron cloud strongly affects the antenna potential in low-density regions such as the solar wind.

As can be seen, a small but easily detectable electric field is present in the diamagnetic cavity. This electric field increases from a few tenths of a millivolt per meter shortly after entry to about 2 mV/m at the exit. As the spacecraft enters the plasma compression region at 1233:15, the electric field abruptly jumps up to about 2.5–3.0 mV/m, occasionally saturating the waveform channel. The electric field stays at about this amplitude until about 1234:00, at which time the field starts to become noisy. At 1234:23 the noise suddenly becomes very intense, saturating the waveform channel. Further details of this intense noise will be discussed in section 6. The electric field remains very noisy for about 1 min and then gradually returns to the strong photoelectron signal characteristic of the undisturbed solar wind.

To further analyze the static electric field signal, it is useful

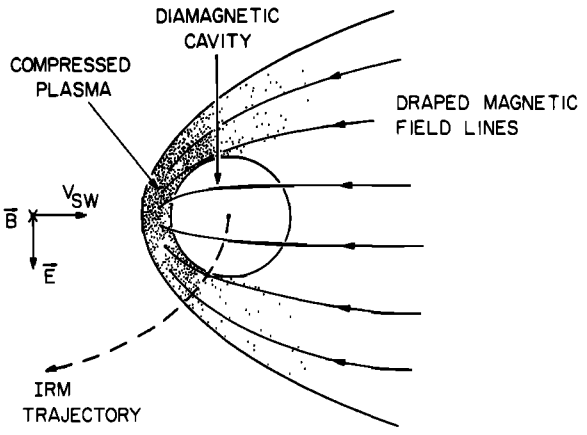

Fig. 3. A schematic diagram showing the diamagnetic ($B = 0$) cavity, the magnetic field lines draped around the cavity, and the compressed plasma upstream of the cavity. The diamagnetic cavity moved in such a way that the IRM followed the trajectory shown by the dashed line.

to introduce a coordinate system called spacecraft-sun coordinates, denoted by a subscript "sc," which stands for spacecraft. In this coordinate system, z_{sc} is parallel to the spacecraft spin axis, the sun is located in the x_{sc}, z_{sc} plane, and y_{sc} completes the right-hand system. This coordinate system is convenient because the measured electric field lies entirely in the x_{sc}, y_{sc} plane, and the unknown field is in the z_{sc} direction. At the time of the December 27, 1984, release the sun was about 4.6° above the x_{sc} axis, with the spin axis directed toward the south and tilted somewhat toward the dawn hemisphere.

Using a least mean-square fitting procedure, the magnitude and direction of the electric field have been determined in the x_{sc}, y_{sc} plane. These parameters are shown in the middle two panels of Figure 4. The angle Φ_E is the azimuthal direction of the electric field measured in the right-hand sense (toward $+y_{sc}$) from the $+x_{sc}$ axis. As can be seen, the angle ϕ_E starts out at about 45°, and then increases to about 90°, where it remains for most of the event. Since the $+x_{sc}$ axis is nearly along the spacecraft-sun line, the electric field is approximately perpendicular to the solar wind velocity.

The existence of a nearly steady electric field in the diamagnetic cavity is quite surprising, since the electric field is expected to be zero in a highly conducting plasma with no magnetic field. We must therefore consider the possibility that the electric field signal is caused by some kind of spacecraft-related effect. Measurements of electric fields using the double-probe technique are notoriously susceptible to spacecraft-induced perturbations, particularly for low plasma densities. The electric field measurement is obtained by measuring the difference in the floating potential of the two antennas. Anything that affects the floating potential differently for the two antennas is a potential source of error. Well-known sources of error include wake effects and asymmetrical photoelectron emission from the spacecraft body. Usually, these errors decrease as the plasma density increases. There are two reasons for this tendency. First, as the plasma density increases, the Debye length becomes smaller, which provides better shielding of the antenna from spacecraft-generated potential perturbations. Second, as the plasma density increases, the incident electron current from the plasma increases, thereby reducing the relative contribution from spacecraft-generated photoelectrons. For a discussion of these and other sources of error, see *Fahleson* [1967]. Experience has shown that double-probe measurements of the type used on the IRM are usually reliable if the electron density is greater than about 10^2–10^3 cm^{-3}. Exceptions can occur when one of the probes is in the optical shadow or geometric wake of the spacecraft body. However, these situations can usually be identified from simple geometric considerations.

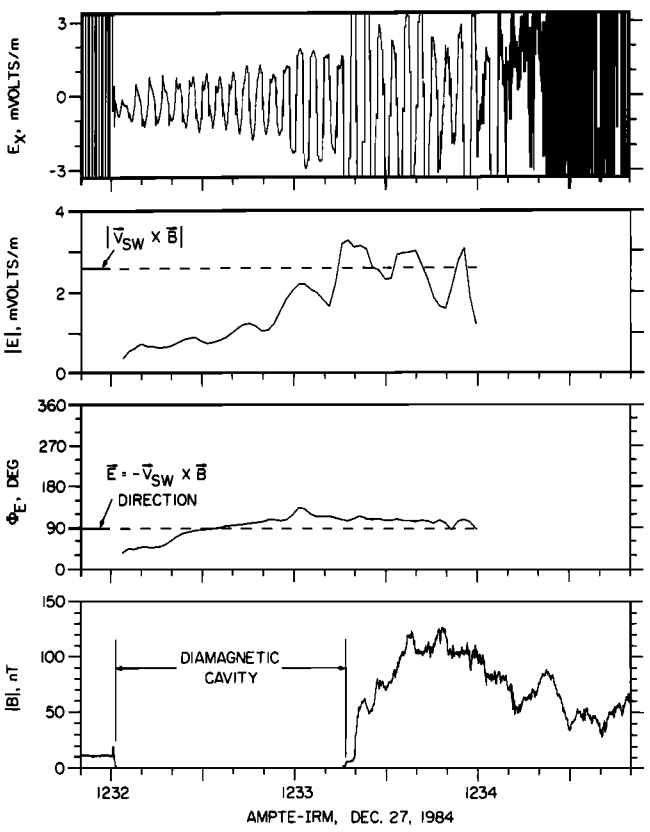

Fig. 4. The quasi-static electric field measurements obtained from the low-frequency waveform channel. The sinusoidal modulation in the top panel is caused by the spacecraft rotation. This modulation can be analyzed to give the magnitude |E| and direction Φ_E of the electric field projected onto the spin plane of the antenna.

The tendency for large errors to develop at low densities is clearly evident in the later stages of the plasma cloud expansion, when the electron density drops below about 10^2 cm^{-3}. However, for the first minute or so after the explosion, the electron densities are well above 10^3 cm^{-3}. For such high densities the double-probe technique should give reliable results. Unfortunately, we have no conclusive test that can clearly determine if the electric field is real. For a real electric field the antenna voltage must vary sinusoidally as the spacecraft rotates. The observed signals provide a reasonably good fit to a sine wave. The antennas are not in the optical shadow of the spacecraft body, and there are no voltage spikes suggesting that the probes are passing through the spacecraft wake. Probably the best indication that the electric field is real is the fact that similar fields were observed during the July 18, 1985, solar wind release, but comparable fields were not observed during the two magnetotail barium releases on March 21 and May 13, 1985. The absence of an electric field during the magnetotail releases would appear to indicate that the electric field is caused by an interaction with the solar wind.

The fact that the electric field is nearly perpendicular to the solar wind velocity suggests a relationship to the convection electric field in the solar wind. To test this hypothesis, we have computed $\mathbf{E} = -\mathbf{V}_{sw} \times \mathbf{B}$ using the magnetic field and solar wind velocity averaged over a 2-min interval just before the event. The computed magnitude and direction, projected onto the x_{sc}, z_{sc} plane, are $|\mathbf{E}| = 2.67$ mV/m and $\Phi_E = 85.4°$. These values are shown by the horizontal dashed lines in the middle two panels of Figure 4. As can be seen, the direction and magnitude of the computed solar wind field are in excellent agreement with the observed field, particularly later in the event. The small deviations could easily be due to changes in the solar wind magnetic field during the event. The magnitude of the electric field is less than the solar wind field early in the event but then starts to return to the solar wind value later in the event. By the time the spacecraft has entered the plasma compression region the electric field has returned almost completely to the solar wind value.

The simplest interpretation of these observations is that some of the solar wind electric field is able to penetrate into the diamagnetic cavity. This interpretation implies that the ion cloud is not able to generate the polarization charges necessary to shield out the external electric field. If a nearly uniform electric field of approximately 11 mV/m exists

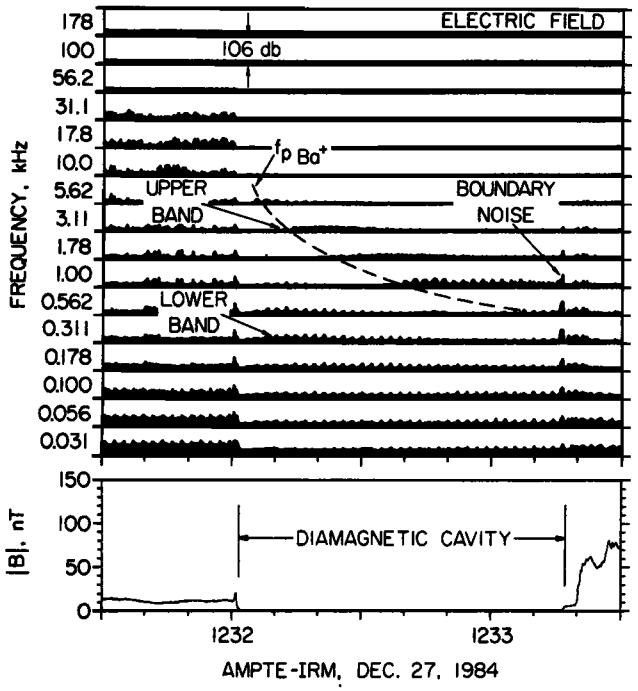

Fig. 5. An expanded 16-channel plot showing the electric field intensities in the diamagnetic cavity. Two distinct emission lines can be seen in the cavity: an upper band near the barium ion plasma frequency f_{pBa^+}, and a lower band well below f_{pBa^+}. Abrupt broadband bursts of noise can also be seen at the boundaries of the diamagnetic cavity.

throughout the cloud, the potential difference across the cloud would be of the order of 100 V. How such a large potential difference could exist across the cloud without producing runaway electrons and large currents is not known.

Another possible interpretation is that the electric field is directed radially outward from the center of the cloud. Since the motion of the cloud is initially perpendicular to the solar wind velocity, this would explain why the field is nearly perpendicular to the spacecraft-sun line. In this interpretation the field would be entirely internal. The association with the solar wind field arises because the motion of the cloud is controlled by the external electric field. A radial electric field is, of course, necessary to confine the faster moving electrons to the ion cloud. The main issue is the magnitude of the field. To confine the electrons, the potential difference between the center of the cloud and the outer boundary must be of the order of the thermal energy of the electrons. For the relatively low electron temperature expected from photoionization, the potential difference should be only a few volts, which is much smaller than the potential difference implied by the electric field measurements. On the other hand, electrons with energies of several hundred electron volts were observed in the ion cloud, apparently caused by some external heating process [*Haerendel et al.*, 1986]. It is possible that the observed electric field could be associated with the confinement of these more energetic electrons. These effects require further study.

4. Waves Inside the Diamagnetic Cavity

Next we describe the waves detected by the IRM inside the diamagnetic cavity. Generally, the wave intensities in the diamagnetic cavity are quite low, much lower than in the solar wind. The wave intensities in the diamagnetic cavity are summarized in Figure 5, which shows the electric field strengths in 16 frequency channels from 31 Hz to 178 kHz. The intensity scale for each channel is logarithmic and covers a dynamic range of 106 dB, from about 0.5 μV/m to 100 mV/m. All 16 frequency channels are sampled once every 0.125 s. Two relatively weak bands of noise can be seen in Figure 5 sweeping downward in frequency with increasing time, the first starting at about 5.62 kHz and sweeping down to about 1 kHz, and the second starting at about 562 Hz and sweeping down to about 178 Hz. Other than the high-frequency electron plasma oscillations described in the previous section, which are not unique to the cavity, these are the only types of waves detected in the diamagnetic cavity. Further details of the two emission bands are given in Figure 6, which shows high-resolution frequency-time spectrograms of the wideband waveform data. The upper band is shown in the top panel, which covers the frequency range from 0 to 10 kHz, and the lower band is shown in the bottom panel, which covers the frequency range from 0 to 1 kHz. The upper band, which is the narrowest, is almost exactly at the barium ion plasma frequency f_{pBa^+}. The

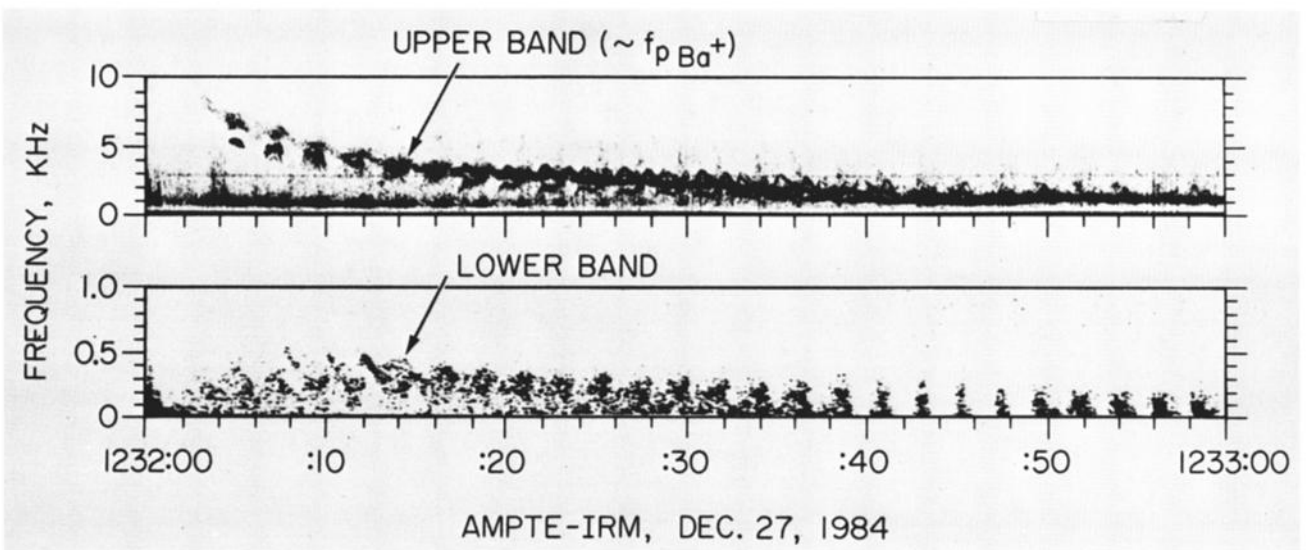

Fig. 6. High-resolution frequency-time spectrograms of the wideband data showing details of the two emission bands observed in the diamagnetic cavity. The upper band is almost exactly at the barium ion plasma frequency f_{pBa^+}.

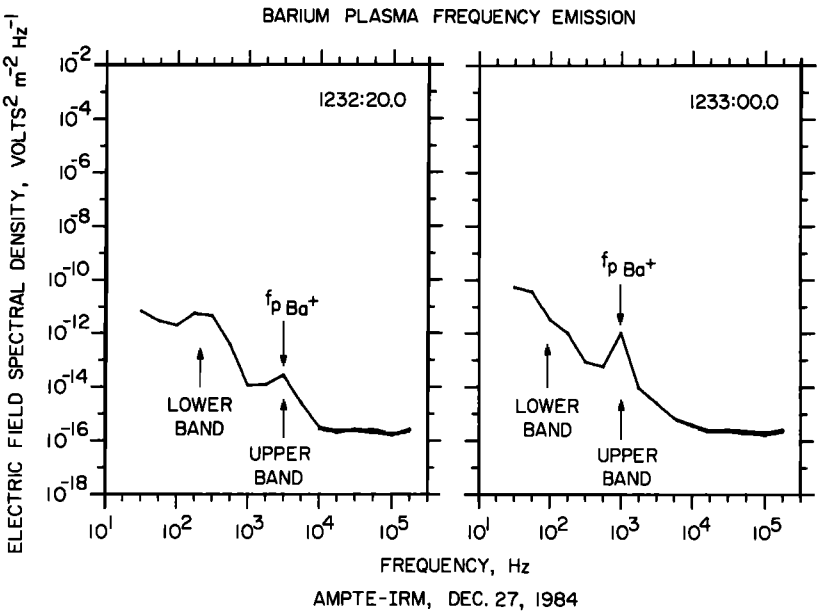

Fig. 7. Selected electric field spectral density plots showing the intensity of the two emission bands observed in the diamagnetic cavity .The barium ion plasma frequency f_{pBa^+} was computed from the electron plasma oscillation line in Plate 1.

ion plasma frequency can be computed by dividing the electron plasma frequency by the square root of the ion to electron mass ratio [*Krall and Trivelpiece*, 1973], which for barium ions is $(m_{Ba}/m_e)^{1/2} = 501$. The relation of the upper band to the ion plasma frequency is further illustrated in Figure 7, which shows two electric field spectrums selected near the beginning and end of the event. As can be seen, the center frequency of the upper band is almost exactly at the barium ion plasma frequency. The lower band is much broader and is about a factor of 10 below the barium ion plasma frequency. The frequency of this band is not simply related to any known characteristic frequency of the plasma. The frequency variation of the lower band is also somewhat different from that of the upper band. The frequency initially increases, reaches a maximum of about 50 Hz at 1232:10, and then decreases slowly, more or less in proportion to the barium ion plasma frequency.

Close examination of the frequency-time spectrograms in Figure 6 shows that the two emission bands have considerable fine structure. Some of this fine structure is modulated at twice the spacecraft spin rate, which is one rotation every 4.4 s. Because the wideband receiver uses an automatic gain control, which tends to maintain a constant signal amplitude, the spin modulation is best studied by using intensity measure-

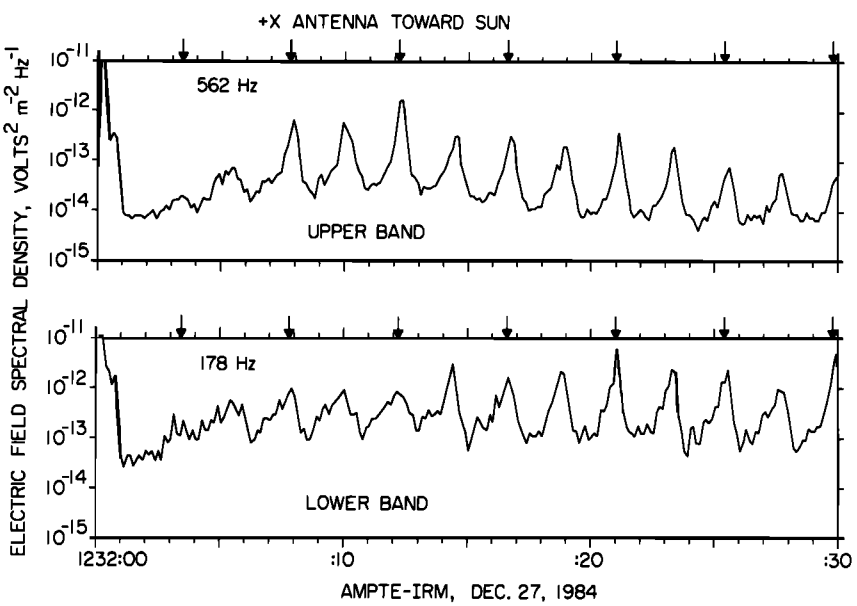

Fig. 8. Expanded intensity plots showing the spin modulation of the two emission bands observed in the diamagnetic cavity. In both cases the intensity is sharply peaked as the antenna axis is aligned approximately along the spacecraft-sun line.

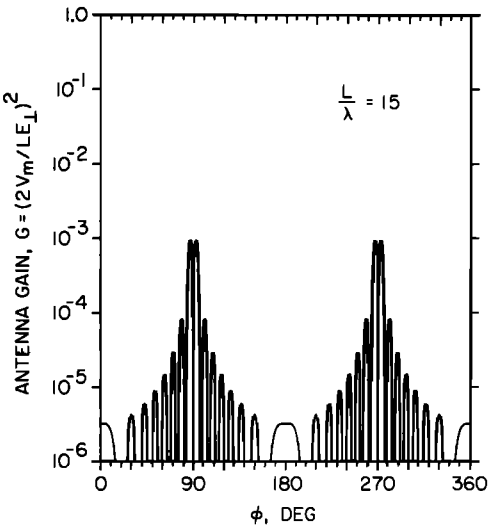

Fig. 9. A plot of the antenna gain as a function of the angle ϕ between the wave vector and the antenna axis for an electrostatic wave with a wavelength λ short in comparison to the antenna length L. The sharply peaked response is believed to account for the sharply peaked spin modulation pattern in Figure 8.

ments from the 16-channel spectrum analyzer. The electric field intensities in the 562-Hz and 178-Hz channels are shown in Figure 8. These channels were selected to illustrate the spin modulation in the upper and lower bands, respectively. Both bands show a sharply defined peak in the electric field intensity when the antenna is aligned approximately along the spacecraft-sun line.

The fact that the spin modulation pattern is sharply peaked has important implications. For long-wavelength electrostatic waves a simple sinusoidal modulation should be observed. Since the modulation is clearly nonsinusoidal, either the wavelength must be short in comparison to the antenna length, thereby producing a nonsinusoidal response, or the emission intensity must be controlled by the spacecraft rotation. The latter would require a spacecraft-related source, such as photoelectrons or some type of wake effect.

First, we will explore the possibility that the spin modulation pattern is caused by wavelengths shorter than the length of the antenna. The response of an electric dipole antenna to short-wavelength electrostatic waves has been studied by *Fuselier and Gurnett* [1984], who showed that the measured antenna voltage is given by

$$v_m = \frac{L}{2}(E_\perp \cos\phi)\left[\frac{\sin x}{x}\right]^2 \tag{1}$$

where

$$x = \frac{k_\perp L}{4}\cos\phi \tag{2}$$

The quantities $E_\perp$ and $K_\perp$ are the projections of the electric field and wave vector onto the spin plane, L is the tip-to-tip length of the antenna, and ϕ is the angle between $\mathbf{E}_\perp$ and $\mathbf{k}_\perp$. This equation assumes that the coupling of the antenna to the plasma is uniform along the length of the antenna. The short-wavelength effects are contained in the sin x/x term. For long wavelengths, $\lambda \gg L$, this term is unity, and the antenna voltage has the usual sinusoidal modulation, as controlled by the cos ϕ term in (1). For short wavelengths, $\lambda \ll L$, the sin x/x term produces a sharply peaked response near $x = 0$, or $\phi = 90°$ and 270°. This effect is illustrated in Figure 9, which shows a plot of the antenna gain factor, $G = (2V_m/LE_\perp)^2$, as a function of ϕ for $L/\lambda = 15$. As can be seen, the envelope of the antenna gain plot is very similar to the spin modulation pattern in Figure 8. The individual nulls are not evident in Figure 8. However, these nulls could easily be smeared out by a small spread in the wave normal direction, or by the finite time constant (0.05 s) of the spectrum analyzer.

If the spin modulation pattern is due to short-wavelength waves, then several conclusions can be made about the nature of these waves. First, the wave vector must be nearly perpendicular to the spacecraft-sun line. This conclusion follows from the antenna gain pattern, which has peaks at $\phi = 90°$ and 270°, and the intensity modulation, which has a maximum along the spacecraft-sun line. Second, the wave vectors must be confined to a narrow range of directions; otherwise, the spin modulation pattern would not be sharply peaked. Third, the electric field strengths must be substantially larger than those given in Figures 7 and 8, because the antenna gain is much less than 1 for short wavelengths. For example, if $L/\lambda = 15$, which gives a reasonable fit to the spin modulation pattern, the peak wave intensities would be a factor of 10^3 higher. The electric field strength of the upper and lower bands would then be about 0.5 mV/m and 1.0 mV/m, respectively.

Next we consider the possible plasma wave modes that could account for the emissions near and below the barium ion plasma frequency. For a plasma with no magnetic field, the only mode that can exist in this frequency range is the ion acoustic mode [*Krall and Trivelpiece*, 1973]. The dispersion relation for the ion acoustic mode is

$$\omega^2 = \frac{C_s^2 k^2}{1 + k^2\lambda_D^2} \tag{3}$$

where k is the wave number, λ_D is the Debye length, and $C_s = (kT_e/m_i)^{1/2}$ is the ion acoustic speed. The characteristic scale length of the ion acoustic mode is the Debye length. For frequencies near the ion plasma frequency the wavelength is of the order of $2\pi\lambda_D$. The Debye length is determined by the electron temperature and electron density [*Krall and Trivelpiece*, 1973]. Since the electrons in the cloud are produced by photoionization, the electron temperature is determined by the solar ultraviolet spectrum and is expected to be about 10^4 °K. For a representative electron density of 10^4 cm^{-3}, $2\pi\lambda_D$ is approximately 0.43 m. This characteristic wavelength is much shorter than the antenna, which is 47 m tip to tip. At frequencies below the ion plasma frequency, the wavelength varies inversely with the frequency: $\lambda = C_s/f$. For a representative electron density of 10^4 cm^{-3}, it is easily verified that the wavelength is less than 47 m for all frequencies above 16 Hz. Since the frequencies observed in the diamagnetic cavity are all above 16 Hz, the wavelengths are in all cases less than the antenna length. These results are consistent with our previous conclusions regarding the wavelength of these waves.

Next we consider the damping of the ion acoustic mode. Equation (3) shows that the wavelength approaches zero as the frequency approaches the ion plasma frequency. Since some of the emissions have frequencies very close to the ion plasma frequency, these waves must have wavelengths comparable to the Debye length. For wavelengths close to the Debye length, Landau damping can be quite important. As is well known [*Krall and Trivelpiece*, 1973], Landau damping is

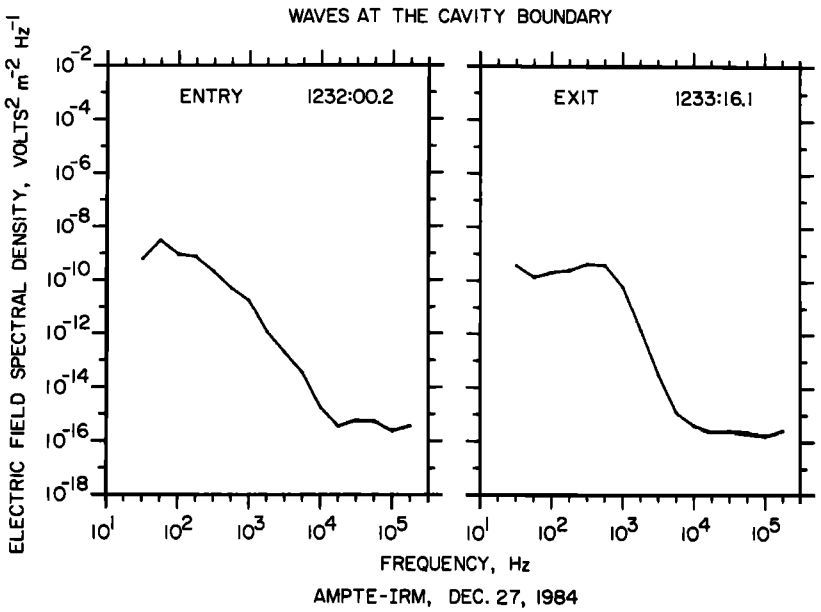

Fig. 10. Electric field spectral density plots showing the spectrum of the noise observed at the boundaries of the diamagnetic cavity. This noise is believed to be caused by ion acoustic waves driven by the electron current flowing along the cavity boundary.

strongly controlled by the electron to ion temperature ratio T_e/T_i. The damping is weak only if $T_e/T_i \gg 1$. Because the ion temperature is controlled by the chemical reaction that produced the barium cloud, the ions are expected to be very cold, not more than about 2000°K initially, and even less as the cloud cools owing to adiabatic expansion. For an electron temperature of 10^4 °K, T_e/T_i is greater than 5. This large electron to ion temperature ratio explains why the waves are not strongly damped.

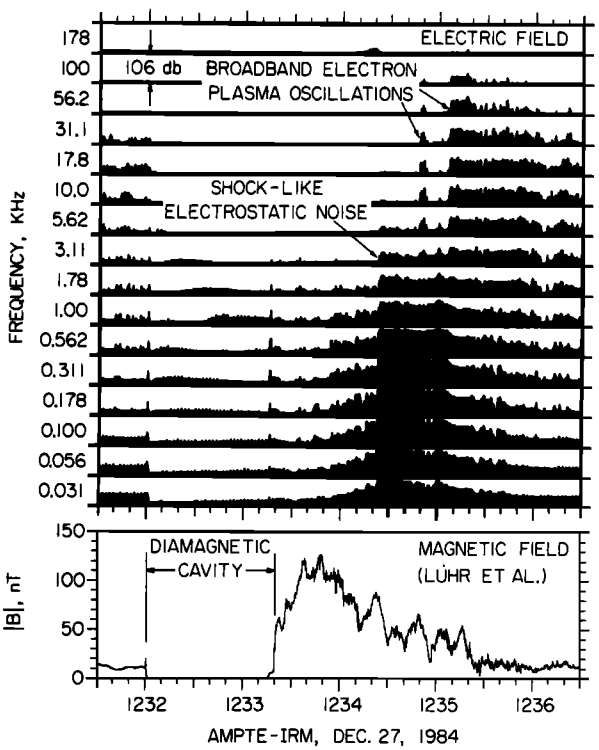

Fig. 11. A 16-channel electric field intensity plot showing the intense electrostatic noise observed near the outer boundary of the plasma compression region, and the broadband electron plasma oscillations in the more distant upstream region.

Finally, we consider the mechanism responsible for generating the waves. The possible mechanisms can be divided into two classes: those involving an interaction of the barium cloud with the solar wind, and those involving an interaction of the spacecraft with the surrounding plasma. Because of the solar wind interaction with the ion cloud there are a number of mechanisms, including currents, beams, and heat fluxes, that could produce ion acoustic waves during the December 27 release. For example, the solar wind proton beam streaming through the cloud could drive an ion acoustic instability. For a discussion of beam-driven ion acoustic instabilities, see *Lemons et al.* [1979]. Also, a variety of electrostatic electron and ion heat flux instabilities exist that could also drive such waves [*Forslund*, 1970; *Gary*, 1978]. The main problem with all of these mechanisms is that similar waves were also observed during the March 21 and May 13, 1985, magnetotail barium releases. These releases show that the waves are not uniquely related to an interaction with the solar wind. The slow drift of the cloud relative to the magnetotail plasma, less than 10 km/s, places severe constraints on any mechanism involving an interaction of the cloud with the surrounding plasma. Because of these difficulties the possibility that the waves might be generated by a spacecraft interaction must be given serious consideration. If the waves have short wavelengths, comparable to the size of the spacecraft, if is possible that photoelectrons from the spacecraft, or some other type of spacecraft-related perturbation, could produce the waves. At present we simply have no clear explanation of the origin of these waves. The possible mechanisms involved require further investigation.

5. Waves at the Cavity Boundary

During both the entry and exit of the diamagnetic cavity, a broadband burst of noise was observed at the cavity boundary. This noise can be seen below about 3.11 kHz at 1232:00 and again at 1233:16 in the spectrogram of Plate 1 and in the

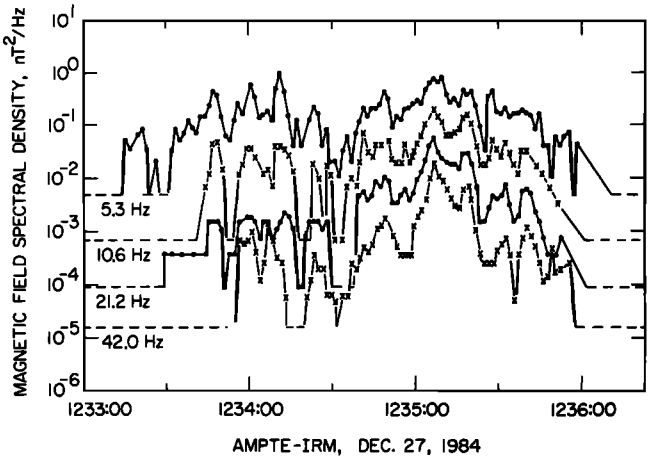

Fig. 12. A plot of the magnetic field spectral density near the plasma compression region. The intense low-frequency magnetic noise occurs in approximately the same region as the intense electrostatic noise.

16-channel plot of Figure 5. Spectrums of this noise, selected from the times of maximum intensity, are shown in Figure 10. The integrated broadband electric field strength is about 0.3 mV/m for the entry, and about 0.4 mV/m for the exit, assuming an antenna gain of 1 ($G = 1$). In both cases the durations are very short, about 0.3 s for the entry, and about 0.5 s for the exit. Using the expansion speed of the cloud, estimated by *Haerendel et al.* [1986] to be 1.7 km/s, the thickness of the unstable layer at the entry into the cavity is estimated to be about 500 m. The corresponding thickness at the exit is more difficult to estimate, because by then the expansion has slowed and the cloud has started to convect but is probably of the order of a few kilometers. As can be seen in Figure 11, the electrostatic noise corresponds almost exactly with the disappearance and return of the magnetic field at the boundaries of the diamagnetic cavity. In both cases the duration of the burst is comparable to the time scale of the magnetic field variation.

The close relationship of the broadband bursts of electrostatic noise to the magnetic field variation strongly suggests that the noise is driven by the electron magnetization current that flows along the boundary of the diamagnetic cavity. The frequency range of the noise, generally below the barium ion plasma frequency, suggests that the noise may also consist of ion acoustic waves. As is well known, ion acoustic waves can be driven by a drift between the electrons and ions, such as must exist at the boundary of the diamagnetic cavity. When the electron temperature is much higher than the ion temperature, as is believed to be the case in the barium cloud, the threshold drift velocity for the ion acoustic instability is quite low, only a few times the ion thermal speed [*Krall and Trivelpiece*, 1973]. For barium ions at a temperature of 2000°K, the ion thermal speed is only about 0.35 km/s. According to the estimates of *Haerendel et al.* [1986] the electrons must be drifting at a velocity of about 13 km/s in order to account for the current at the cavity boundary. This drift velocity greatly exceeds the threshold drift velocity, indicating that the ion acoustic mode should be unstable.

6. Waves Associated With the Compression Region

The wave intensities outside the diamagnetic cavity are shown in the 16-channel electric field plot of Figure 11. After leaving the diamagnetic cavity as 1233:16 and entering the plasma compression region the electric field intensities drop to very low levels. Except for a few weak sporadic bursts the electric field intensities remain at a low level until about 1233:55, where they gradually begin to increase. At about 1234:23, near the outer boundary of the compression region the electric field intensities suddenly increase to very high levels, so high that they saturate some channels of the spectrum analyzer. This very intense noise corresponds to the red region of the spectrogram marked "electrostatic noise" in Plate 1. The noise is electrostatic because it extends well above the electron cyclotron frequency, in a region where no electromagnetic mode exists. After about 1235:10 the electric field

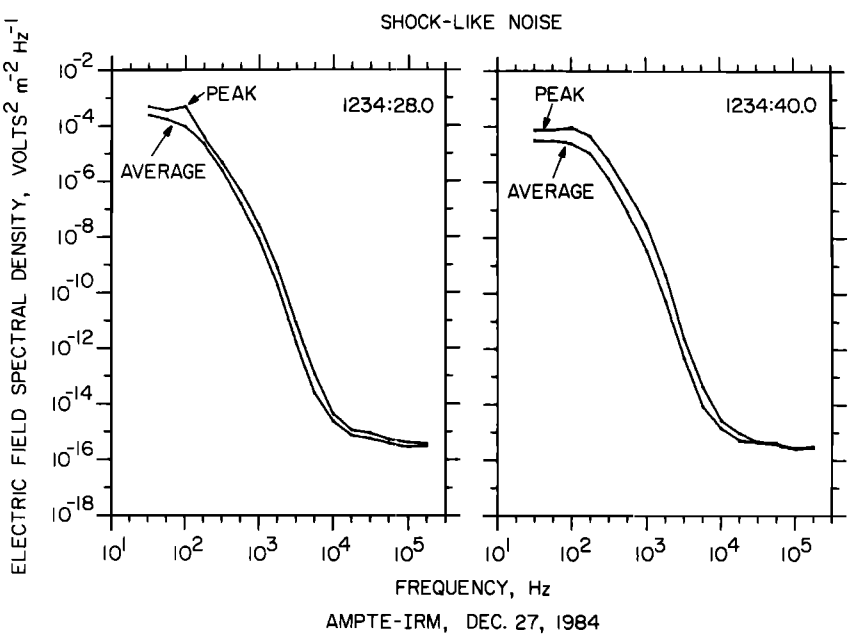

Fig. 13. Selected electric field spectrums of the intense electrostatic noise. Most of the power in this noise is concentrated at frequencies below a few hundred hertz.

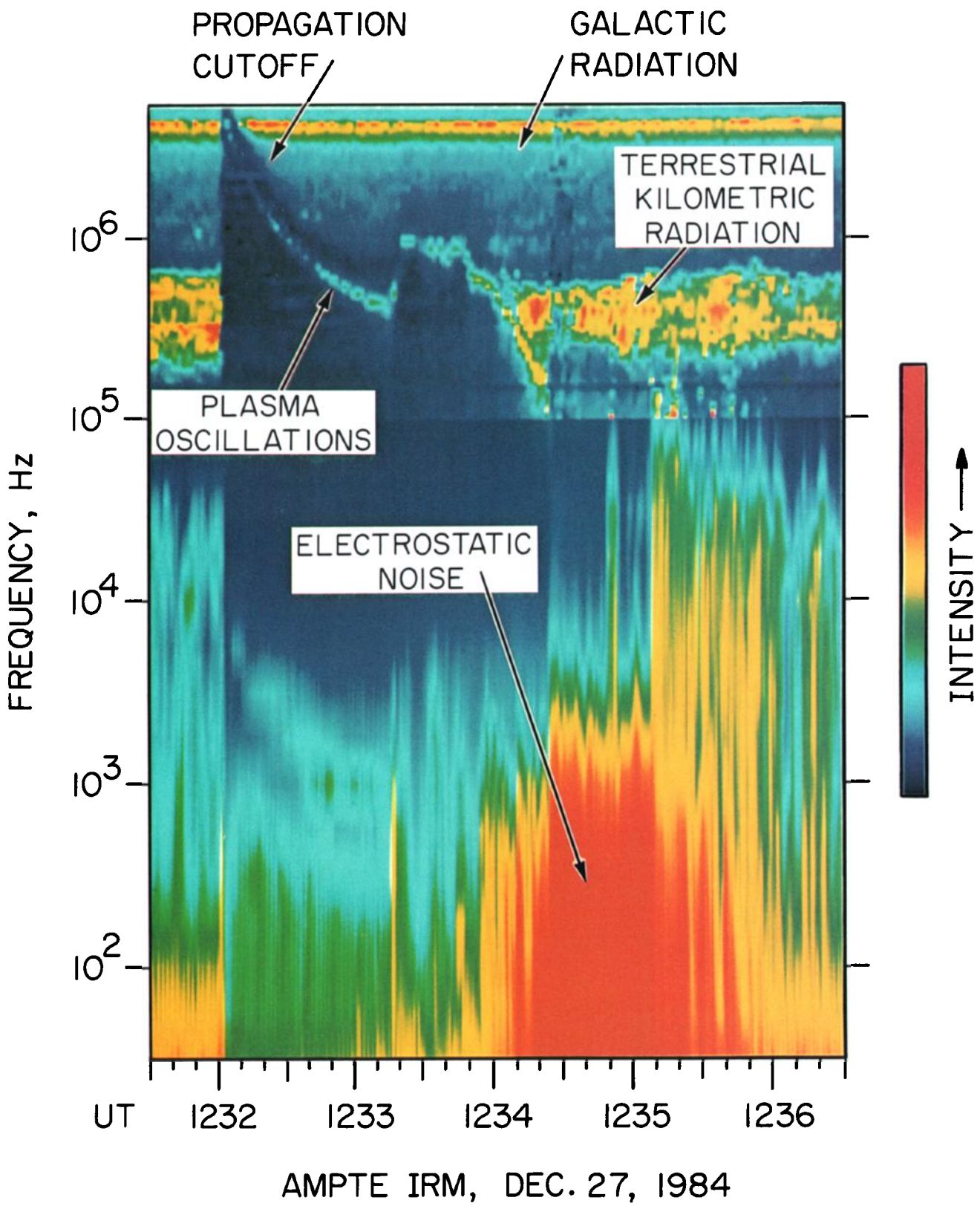

Plate 1. A frequency-time spectrogram from the high-frequency sweep-frequency receiver. The intensity scale is adjusted as a function of frequency so that the dynamic range extends from the instrument noise level (blue) to the saturation level (red). The dense plasma cloud formed by the explosion at 1232:00 blocked the galactic and terrestrial radio noise and produced depressed noise intensities for about 2 min as the cloud expanded over the spacecraft. The electron number density N_e can be determined from the electron plasma oscillation line, which is at the local electron plasma frequency f_{pe}, $= 9000\,(N_e)^{1/2}$ Hz, where N_e is in cm^{-3}.

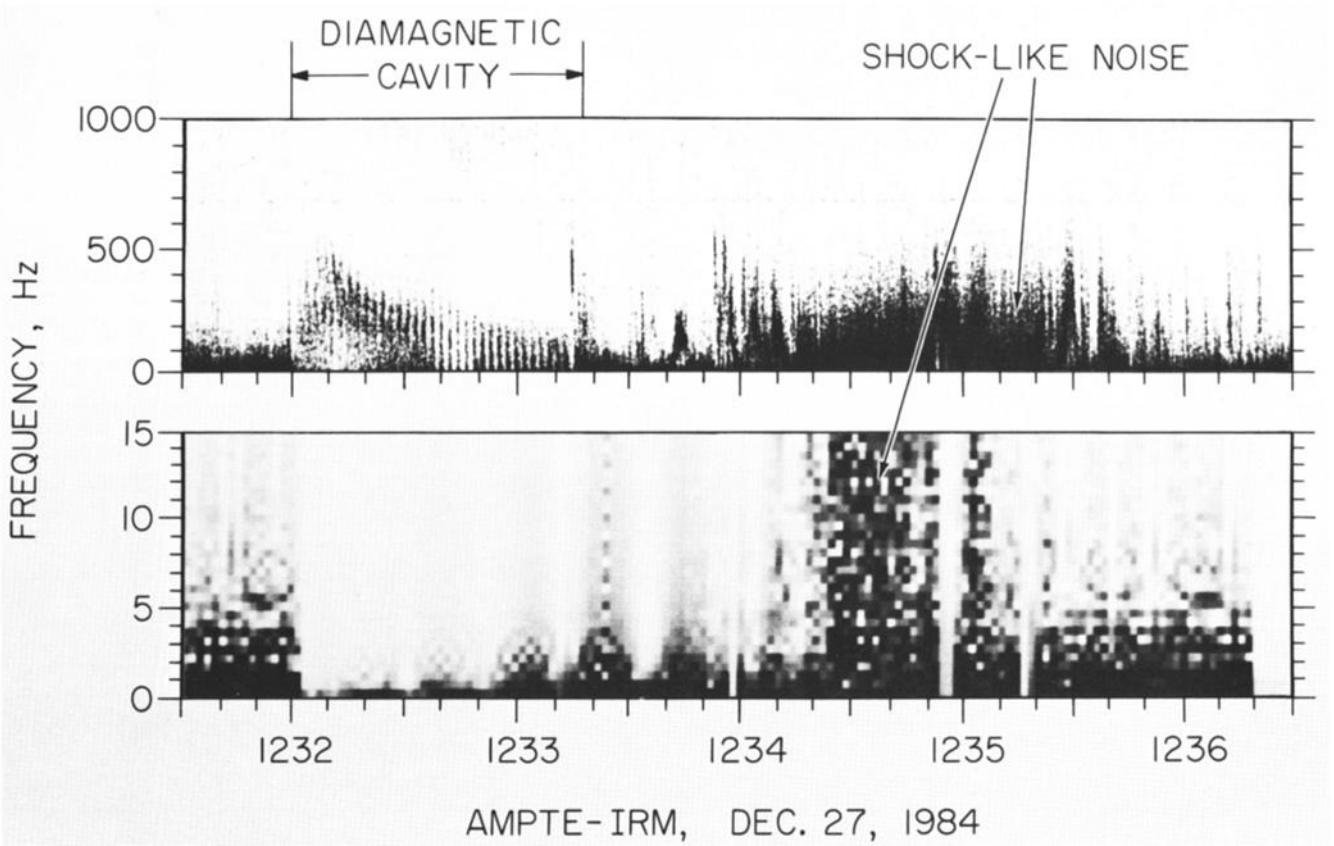

Fig. 14. Wideband electric field spectrograms of the intense electrostatic noise. The spectrum of the electrostatic noise is relatively featureless, with no evidence of lines near either the electron cyclotron frequency or the lower hybrid resonance frequency.

intensities begin to decrease, gradually decreasing to the ambient solar wind level over a period of about 1 min. Low-frequency magnetic field measurements, given in Figure 12, show that this same interval, from about 1234:23 to 1235:10, is also characterized by very high magnetic noise levels. This magnetic noise is at frequencies below the electron cyclotron frequency, in a region where electromagnetic waves can propagate.

Representative electric field spectrums of the intense electrostatic noise are shown in Figure 13. The spectrums typically show a flat plateau at low frequencies, with a rapid decrease in intensity at frequencies above a few hundred hertz. Sometimes a slight peak or enhancement is evident near 100 Hz. At maximum intensity the broadband electric field strength, integrated over all the frequency channels, is 140 mV/m, and may be even higher because some of the channels are saturated. These electric field intensities are among the most intense ever recorded by a space plasma wave experiment. Wideband spectrograms of the electric field waveform, illustrated in Figure 14, show that the spectrum is relatively featureless. In particular, there is no evidence of emissions near the electron cyclotron frequency f_{ce} or the lower hybrid resonance frequency $f_{LHR} = (f_{ce} f_{ci})^{1/2}$. The lower hybrid frequency should be in the range from a few hertz to a few tens of hertz, depending on the plasma composition. Also, no evidence of spin modulation can be seen in the electric field intensity, indicating that the waves responsible for the noise are generated over a broad range of wave normal directions.

Proceeding farther upstream, another type of higher-frequency electric field noise can be seen in Figure 11 starting at about 1235:05. Two representative spectrums of this upstream noise are shown in Figure 15. The upstream noise is characterized by a broad peak extending from about 3 to 30 kHz, somewhat below the electron plasma frequency. After the initial sharp onset, the center frequency and intensity of the noise tend to decrease with increasing time. Occasionally, a sharp peak can be seen in the spectrum, as at 1235:40 in Figure 15. This peak is believed to be at the local electron plasma frequency.

The existence of the intense electrostatic noise near the outer boundary of the compression region raises an important question as to whether this noise and the related plasma effects are caused by a collisionless shock. This question was first considered by *Gurnett et al.* [1986] in the interpretation of the AMPTE solar wind lithium releases and was motivated by the fact that the electrostatic noise has a spectrum very similar to the electrostatic noise observed in the earth's bow shock [*Fredricks et al.*, 1968, 1970*a*, *b*; *Rodriguez and Gurnett*, 1975; *Gurnett*, 1985]. If the effects observed upstream of the artificial comet are to be interpreted as a shock, then certain basic conditions must be satisfied. The first requirement for a shock is that the plasma must have a component of flow across the discontinuity. It is quite clear that the solar wind plasma flows continuously through this region. This fact is illustrated in the top panel of Figure 16, which shows an energy-time spectrogram of ions arriving from the direction of the sun. The dark band across the spectrogram at an energy of about 200–500 eV is due to solar wind protons. As can be seen, the flux of solar wind protons is essentially continuous through the entire event. The second requirement for a shock

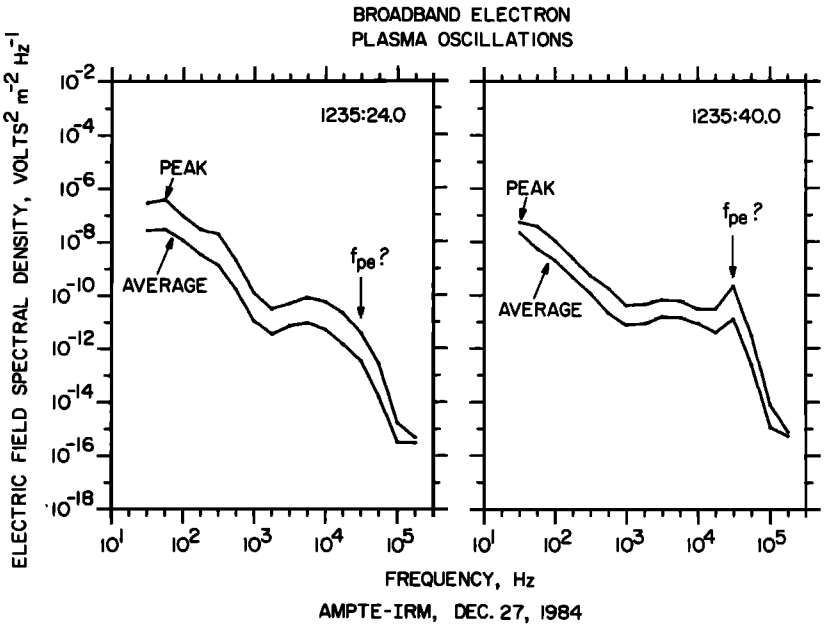

Fig. 15. Electric field spectrums showing the spectrum of the broadband electron plasma oscillations observed in the upstream region. The spectrum of these emissions is very broad and is shifted downward somewhat below the electron plasma frequency.

is that the magnetic field and plasma density must increase and the flow velocity must decrease as the plasma flows across the discontinuity. Remembering that the spacecraft is moving upstream in relation to the ion cloud, comparison of Figures 1 and 11 clearly shows that in a frame of reference moving with the solar wind plasma the magnetic field and plasma density both increase in the region where the intense electrostatic noise occurs. The region of increasing magnetic field, from about 1235:25 to 1233:45, corresponds almost exactly to the region of intense noise. The region of increasing plasma density is less well defined, since the upstream boundary cannot be determined (see Figure 1). However, it is clear that the plasma density increase also occurs in the same general region where the noise is observed. The second panel from the bottom in Figure 16 also shows that the solar wind proton speed decreases from about 1235:30 to 1233:20, again in the same general region where the electrostatic noise is observed. The reduction in the bulk flow velocity is probably even more pronounced that is indicated by the proton speed, because the plasma instrument does not detect the barium ions, which are nearly at rest with respect to the spacecraft. The third and final requirment for a shock is that the entropy must increase as the plasma flows across the shock. Whether this condition is satisfied cannot be answered quantitatively because the plasma instrument does not have sufficient resolution to accurately measure the plasma temperature. However, as can be seen in the middle and bottom panels of Figure 16, the plasma is being heated in the region where the noise occurs. This heating provides strong qualitative evidence that the entropy is increasing. Although it is not certain that the highly turbulent transition region upstream of the ion cloud is a shock, it certainly has many features similar to a shock.

Next we consider the origin of the intense electrostatic noise in the turbulent transition region. Our present view is that the noise is caused by an ion beam-plasma interaction between the nearly stationary barium ions and the rapidly moving solar wind protons. The essential elements of this instability were discussed by *Gurnett et al.* [1986] in the analysis of the AMPTE solar wind lithium releases. The reduced one-dimensional distribution function assumed in this model is shown in Figure 17. Because the barium ions are born at rest, these ions are represented by a Maxwellian centered on zero velocity. The barium ions are assumed to be at a temperature of 2×10^3 °K. This temperature is probably an upper limit, because the ions cool as the cloud expands. Lower ion temperatures tend to make the instability even stronger. The solar wind protons are represented by a Maxwellian centered on the solar wind velocity V_{sw}, which is taken to be 500 km/s. The solar wind proton temperature is assumed to be about 10^5 °K, which is typical of the solar wind near 1 AU. Two classes of electrons must be considered, relatively cold, $\sim 10^4$ °K, electrons from the photoionization of barium, and much hotter, $\sim 5 \times 10^5$ °K, solar wind electrons, which have been heated somewhat in the vicinity of the cloud. Both classes of electrons are represented by Maxwellians. Because the cyclotron radius of the electrons is expected to be small in comparison to the radius of the cloud, the two electron components are assumed to have the same $\mathbf{E} \times \mathbf{B}$ drift velocity, V_d. The drift velocity is adjusted so that the net current in the plasma is zero. This last condition is based on the fact that the magnetic field measurements show that the net current in the plasma is small in comparison to the current contributed by the beam of solar wind protons.

Two types of beam-plasma instabilities can occur in this type of plasma, one with phase velocities between the barium ions and the electrons, $0 < \omega/k < V_d$, and the other between the electrons and the solar wind protons, $V_d < \omega/k < V_{sw}$. Of these, only the instability associated with the barium ions is important. The reason is that the instability is strongly influenced by the electron to ion temperature ratio. Because the barium ions are much colder than the protons, the instability associated with the barium ions has a much lower threshold. The growth rate of the ion beam-plasma instability is also strongly controlled by the relative density of the barium ions

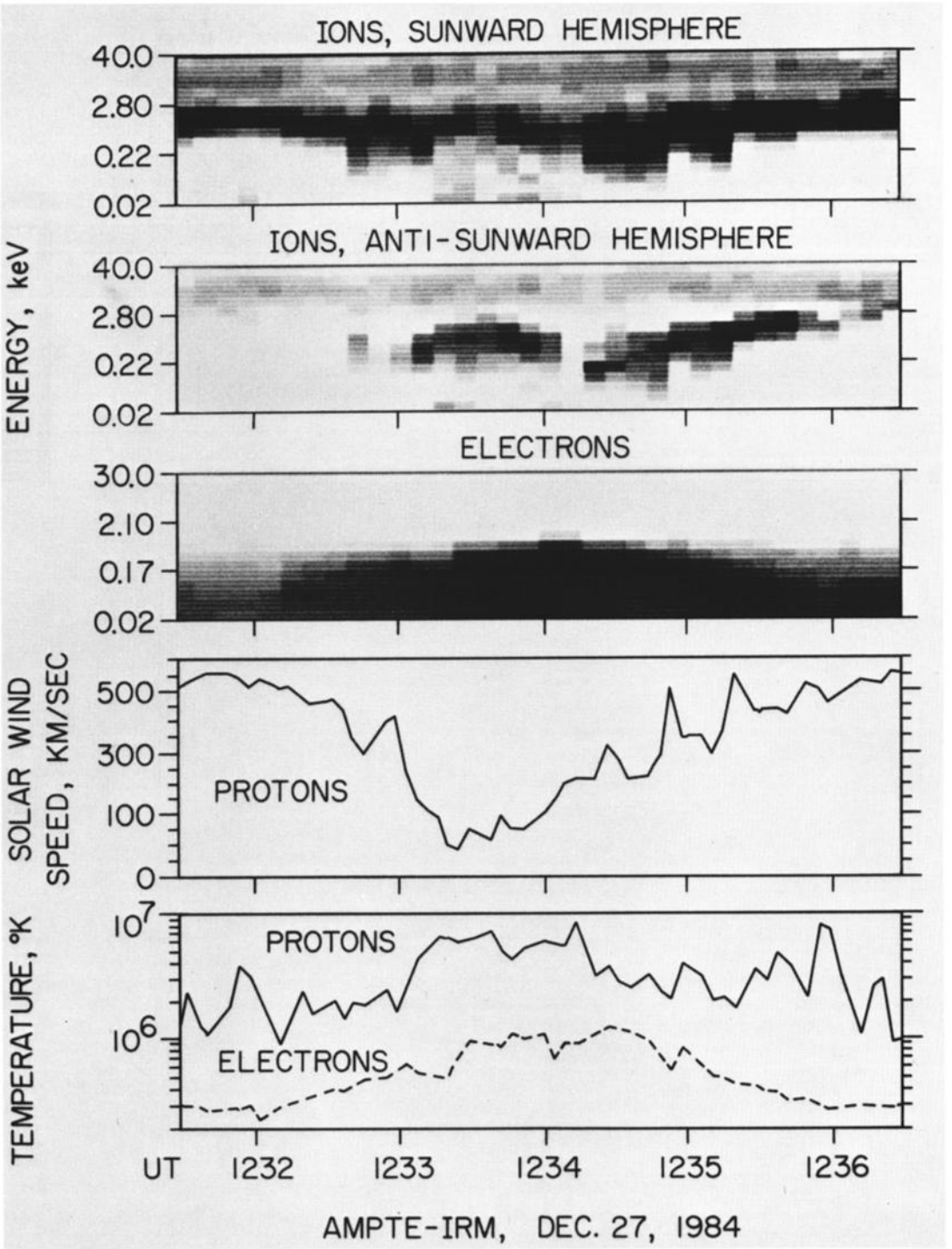

Fig. 16. Energy-time spectrograms and selected bulk parameters from the plasma instrument. The top panel shows that the solar wind proton stream was observed continuously throughout the event. The ions detected in the antisunward viewing hemisphere from about 1234:10 to 1236:00 are believed to be barium ions accelerated by the solar wind electric field. These ions are observed during the same time that the intense electrostatic noise is observed.

and the protons. Instability only occurs if the two ion species have somewhat similar densities. Otherwise, the instability associated with the minority ion disappears because the "beam" density is too low, and the instability associated with the majority ion disappears because the drift velocity with respect to the electrons is too low. This density dependence explains why the electrostatic noise is only observed near the outer boundary of the ion cloud. It is only in this region (see Figure 1) that the barium ion and proton densities are sufficiently similar for the instability to occur.

Because the ion beam-plasma instability has been previously analyzed for a solar wind lithium release [*Gurnett et al.*, 1986], we will only present a summary of the corresponding analysis for the December 27 barium release. Figure 18 shows the frequency of the marginal stability boundary ($\gamma = 0$) plotted as a function of the barium ion to proton density ratio. This analysis uses the previously mentioned temperatures and velocities and assumes that the cold photoelectron density is equal to the barium ion density. Although the cold photoelectron density cannot be directly measured, it has been pre-

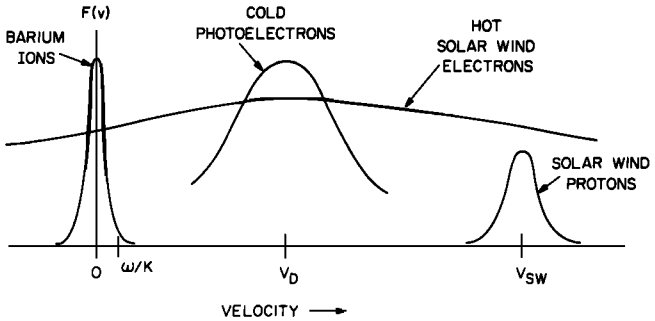

Fig. 17. A schematic illustration of the reduced one-dimensional velocity distribution believed to be responsible for the intense electrostatic noise. The basic instability is believed to occur at phase velocities ω/k between the barium ions and the electrons. The electrons are assumed to drift at a velocity V_d such that the net current is zero.

viously shown [*Gurnett et al.*, 1986] that the results are relatively insensitive to this parameter. The marginal stability plot shows that electrostatic waves are unstable for frequencies up to about 350 Hz, and for barium ion to proton density ratios from about 2.2×10^{-2} to 2.6×10^{2}. The observed frequency range of the electrostatic noise, up to a few hundred hertz (see Figure 13), and the onset of the electrostatic noise, at a density ratio of $N_{Ba^+}/N_p \simeq 10^2$ (see Figures 1 and 11), are in good agreement with the predictions of the model. Unfortunately, the lower bound for the density ratio cannot be compared because the barium ion density cannot be accurately determined after about 1234:30.

Detailed calculations of the wave number and growth rate for a representative set of parameters are shown in Figure 19. The top panel shows that the wavelengths produced are very short ($k\lambda_D \sim 0.1$). The wavelengths are much shorter than either the electron or ion cyclotron radii, which justifies ignoring the static magnetic field. The phase and group velocities are about 25 km/s. The bottom panel of Figure 19 shows the growth rate as a function of frequency. The maximum growth rate is about 10 s^{-1}. Assuming the scale size to be about 100 km, the waves take about 4 s to propagate through the unstable region, which gives an amplitude increase of e^{40}. The

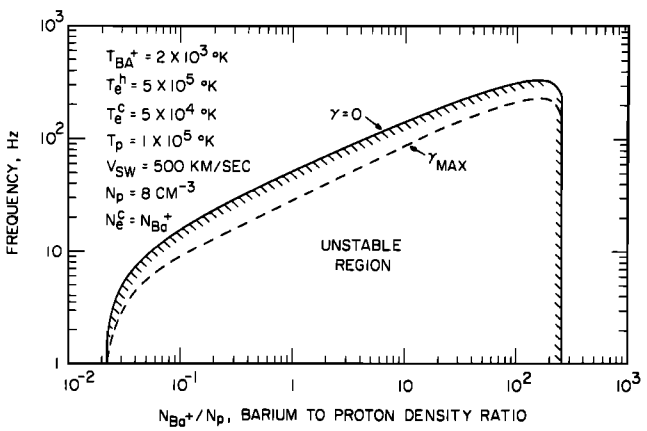

Fig. 18. The marginal stability boundary ($\gamma = 0$) and maximum growth rate (γ_{max}) of the ion beam-plasma instability as a function of frequency and the barium ion to proton density ratio N_{Ba^+}/N_p. Note that the instability only occurs for a limited range of N_{Ba^+}/N_p. This explains why the noise is confined to a relatively limited region near the outer boundary of the plasma compression region.

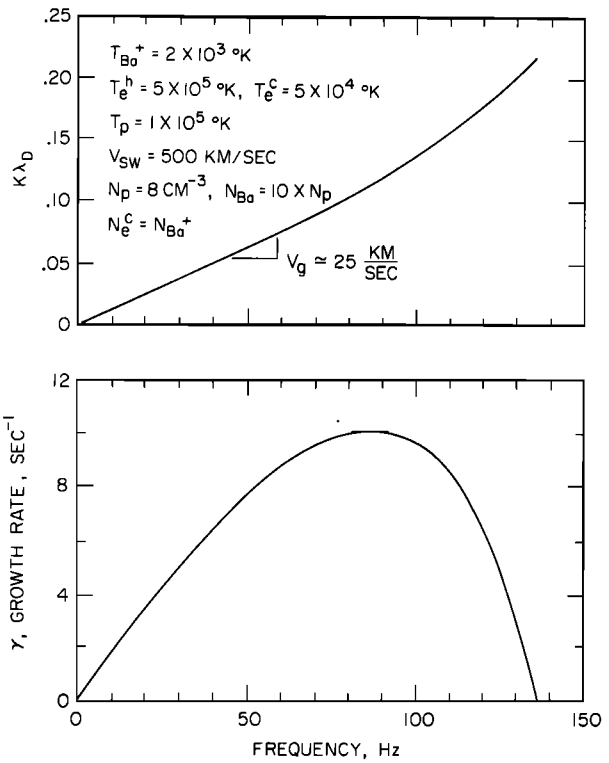

Fig. 19. The growth rate γ and wave number k of the ion beam-plasma instability as a function of frequency for a representative set of parameters. The maximum growth rate in this case occurred at a frequency of 90 Hz, and a wave number of $k\lambda_D \simeq 0.1$.

growth rates are threfore more than adequate to explain the generation of intense noise. Although the basic model is one-dimensional, the results can be easily extended to waves propagating at an arbitrary angle [*Krall and Trivelpiece*, 1973]. An analysis for arbitrary propagation directions is under way (T. Z. Ma et al., unpublished manuscript, 1986).

Before concluding the analysis of the ion beam-plasma instability, it is useful to discuss the possible role of barium ions accelerated by the solar wind electric field. The second panel from the top in Figure 16 shows two distinct ion populations that are well separated from the solar wind protons. One of these components, from about 1234:10 to 1236:00, is believed to consist of barium ions that have been accelerated by the solar wind electric field [*Haerendel et al.*, 1986]. The energy of this component increases with increasing time, starting at a few tens of eV and eventually reaching several keV. The energy is believed to increase because the path length available for acceleration increases as the cloud moves away from the spacecraft. As can be seen by comparing with Figure 11, the accelerated barium ions are observed over almost exactly the same interval as the intense electrostatic noise, suggesting that the accelerated barium ions may be responsible for the electrostatic noise. This relationship is believed to be largely coincidental. Even at energies of several keV the barium velocities are still much less than the solar wind velocity. Therefore the velocity of the accelerated barium ions is small and should have little effect on the stability analysis. Furthermore, the acceleration is nearly perpendicular to the solar wind velocity, which minimizes the effect on the one-dimensional distribution function projected along the solar wind velocity direction.

In addition to the intense electrostatic noise, the low-

frequency magnetic noise and the high-frequency electrostatic noise also require analysis. At the present time we have not undertaken a detailed analysis of either of these types of noise. It is our impression that the low-frequency magnetic noise may be due to an electromagnetic ion beam instability, possibly similar to the instability responsible for low-frequency ULF waves upstream of the earth's bow shock [*Gary et al.*, 1981; *Winske and Leroy*, 1984], with the barium ions playing the same role as upstream ion beams. As discussed earlier, the high-frequency electrostatic noise appears to be associated with the electron plasma frequency. It seems likely that these waves are electron plasma oscillations that are downshifted in frequency, similar to the waves described by *Fuselier et al.* [1985] upstream of the earth's bow shock. For beam energies near the electron thermal speed the frequency range of the Langmuir mode is broadened and shifted downward in frequency below the electron plasma frequency. At present it is not known whether an appropriate beam is present or not. The electron energy spectrum in the middle panel of Figure 16 does not show any evidence of such a beam, although *Rodgers et al.* [1986] did detect an electron beam at the UKS spacecraft during this same interval. It is also possible that barium ions upstream of the cloud could provide a suitable "beam" for driving this instability.

7. CONCLUSIONS

The plasma waves and electric fields observed during the artificial comet experiment showed many similarities and several notable differences with the previous solar wind lithium releases. The electron density profile obtained during the barium release was much clearer and better defined, with a substantially higher peak density. This is due to the more rapid ionization of barium, which produced a much denser ion cloud. The higher density and longer duration also provided a much better determination of the static electric field in the diamagnetic cavity .The static electric field measurements show the existence of an electric field of ~ 1 mV/m in the diamagnetic cavity. This field is in the same direction as the solar wind convection electric field, which suggests that the solar with field is able to partially penetrate into the cloud. How such a large electric field can exist in an essentially collisionless plasma without causing large disruptive effects is not known. The observation of an electrostatic emission line at the barium ion plasma frequency is a new effect that was largely unanticipated. Subsequent analysis of the lithium releases [*Häusler et al.*, 1986] reveals that a similar emission line was probably also present at the lithium ion plasma frequency, although the emission is not nearly as clear or well defined as in the barium release. Analysis of the spin modulation of these emissions strongly indicates that this noise is caused by waves with very short wavelengths, probably ion acoustic waves. The free energy source for these waves still has not been clearly established. Outside the diamagnetic cavity, the most notable plasma wave effect was the very intense electrostatic noise detected near the outer boundary of the plasma compression region. This noise is similar to the noise observed upstream of the lithium cloud, but more intense. The question again arises as to whether this noise is indicative of a shocklike interaction between the ion cloud and the solar wind. Although it is not certain that this highly turbulent region is a shock, it certainly has many characteristics similar to a shock. As in the lithium release it seems reasonably certain that the intense electrostatic noise is caused by a beam-plasma interaction between the nearly stationary barium ions and the rapidly moving solar wind protons. The possible role of this noise in heating the plasma needs further investigation.

This experiment showed many interesting new plasma effects associated with neutral gas injections in rapidly moving plasmas. Some of these effects, particularly the turbulent wave-particle interactions on the upstream side of the ion cloud, are relevant to natural comets, where similar types of instabilities are observed [*Scarf et al.*, 1986].

Acknowledgments. We wish to thank Gracen Joiner of the Office of Naval Research (ONR) for his invaluable support, without which we would not have been able to carry out this project. We also thank D. Odem of the University of Iowa, W. B. Harbridge of Aerospace Corporation, and K. Gnaiger and F. Eberl of the Max-Planck-Institut für extraterrestrische Physik for valuable technical suport. The research at the University of Iowa was supported by ONR contracts N00014-82-K-0183 and N00014-85-K-0404, and NASA grants NGL-16-001-002 and NGL-16-001-043. The research at the Aerospace Corporation was supported in part by ONR contract N00014-84-K-0160 and in part by the U.S. Air Force Systems Commands Space Division under contract F04701-84-C-0085. The research at The University of Washington was supported by ONR contract N00014-84-K-0160.

The Editor thanks M. B. Pongratz and E. P. Szuszczewicz for their assistance in evaluating this paper.

REFERENCES

Adamson, D., C. L. Fricke, S. A. T. Long, W. F. Landon, and D. L. Ridge, Preliminary analysis of NASA optical data obtained in barium ion cloud experiment of September 21, 1971, *J. Geophys. Res.*, *78*, 5769, 1973.

Biermann, L., R. Lüst, Rh. Lüst, and H. U. Schmidt, Zur Untersuchung des interplanetaren Mediums mit Hilfe künstlich eigenbrachter Ionenwolken, *Z. Astrophys.*, *53*, 226, 1961.

Carlsten, J. L., Photoionization of barium clouds via the ^3D metastable levels, *Planet. Space Sci.*, *23*, 53, 1975.

Fahleson, U. V., Theory of electric field measurements conducted in the magnetosphere with electric probes, *Space Sci. Rev.*, *7*, 238, 1967.

Föppl, H., G. Haerendel, L. Haser, R. Lüst, F. Melzner, N. Neuss, H. H. Rabben, E. Rieger, J. Stöcker, and W. Stoffregen, Preliminary results of electric field measurements in the auroral zone, *J. Geophys. Res.*, *73*, 21, 1968.

Forslund, D. W., Instabilities associated with heat conduction in the solar wind and their consequences, *J. Geophys. Res.*, *75*, 17, 1970.

Fredricks, R. W., C. F. Kennel, F. L. Scarf, G. M. Crook, and I. M. Green, Detection of electric-field turbulence in the earth's bow shock, *Phys. Rev. Lett.*, *21*, 1761, 1968.

Fredricks, R. W., F. W. Coroniti, C. F. Kennel, and F. L. Scarf, Fast-resolved spectra of electrostatic turbulence in the earth's bow shock, *Phys. Rev. Lett.*, *24*, 994, 1970*a*.

Fredricks, R. W., G. M. Crook, C. F. Kennel, I. M. Green, F. L. Scarf, P. J. Coleman, and C. T. Russell, OGO 5 observations of electrostatic turbulence in bow shock magnetic structures, *J. Geophys. Res.*, *75*, 3751, 1970*b*.

Fuselier, S. A., and D. A. Gurnett, Short wavelength ion waves upstream of the earth's bow shock, *J. Geophys. Res.*, *89*, 91, 1984.

Fuselier, S. A., D. A. Gurnett, and R. J. Fitzenreiter, The downshift of electron plasma oscillations in the electron foreshock region, *J. Geophys. Res. 90*, 3935, 1985.

Gary, S. P., Electrostatic heat flux instabilities, *J. Plasma Phys. 20*, 47, 1978.

Gary, S. P., J. T. Gosling, and D. W. Forslund, The electromagnetic ion beam instability upstream of the earth's bow shock, *J. Geophys. Res.*, *86*, 6691, 1981.

Gurnett, D. A., Plasma waves and instabilities, in *Collisionless Shocks in the Heliosphere: Reviews of Current Research, Geophys Monogr. Ser.*, vol. 35, edited by B. T. Tsurutani and R. G. Stone, p. 207, AGU, Washington, D. C., 1985.

Gurnett, D. A., R. R Anderson, B. Häusler, G. Haerendel, O. H. Bauer, R. A. Treumann, H. C. Koons, R. H. Holzworth, and H. Lühr, Plasma waves associated with the AMPTE artificial comet, *Geophys. Res. Lett.*, *12*, 851, 1985.

Gurnett, D. A., T. Z. Ma, R. R. Anderson, O. H. Bauer, G. Haerendel, B. Häusler, G. Paschmann, R. A. Treumann, H. C. Koons, R. Holzworth, and H. Lühr, Analysis and interpretation of the shock-like electronstatic noise observed during the AMPTE lithium releases, *J. Geophys. Res.*, *91*, 1301, 1986.

Haerendel, G., Plasma confinement and interaction experiment, Active Experiments in Space, *Eur. Space Agency Spec. Publ., ESA SP-196*, 337, 1983.

Haerendel, G., and R. Lüst, Artificial plasma clouds in space, *Sci. Am.*, *219*, 80, 1968.

Haerendel, G., R. Lüst, and E. Rieger, Motion of artificial ion clouds, *Planet. Space Sci.*, *15*, 1, 1967.

Haerendel, G., E. Rieger, A. Valenzuela, H. Föppl, H. C. Stenbaek-Nielsen, and E. M. Wescott, First observations of electrostatic acceleration of barium ions into the magnetosphere, *Eur. Space Agency Spec. Publ., ESA SP-115*, 1976.

Haerendel, G., G. Paschmann, W. Baumjohann, and C. W. Carlson, Dynamics of the AMPTE artificial comet, *Nature*, *320*, 22, 1986.

Häusler, B., R. R. Anderson, D. A. Gurnett, H. C. Koons, R. H. Holtzworth, O. H. Bauer, R. Treumann, K. Gnaiger, D. Odem, W. B. Harbridge, and F. Eberl, The plasma wave instrument onboard the AMPTE-IRM spacecraft, *IEEE Trans. Geosci. Remote Sens.*, *GE-23*, 267, 1985.

Häusler, B., L. J. Wolliscroft, R. R. Anderson, D. A. Gurnett, R. H. Holzworth, H. C. Koons, O. H Bauer, G. Haerendel, R. A. Treumann, P. J. Christiansen, A. G. Darbyshire, M. P. Gough, S. R. Jones, A. J. Norris, H. Lühr, and N. Klöcker, Plasma waves observed by the IRM and UKS spacecraft during the AMPTE solar wind lithium releases: Overview, *J. Geophys. Res.*, *91*, 1283, 1986.

Heppner, J. P., J. D. Stolarik, and E. M. Wescott, Electric field measurements and the identification of currents causing magnetic disturbances in the polar cap, *J. Geophys. Res.*, *76*, 6028, 1971.

Kintner, P. M., M. C. Kelley, G. Holmgren, and R. Bostrom, The observation and production of ion acoustic waves during the trigger experiment, *J. Geophys. Res.*, *85*, 5071, 1980.

Koons, H. C., and M. B. Pongratz, Ion cyclotron waves generated by an ionospheric barium injection, *J. Geophys. Res.*, *84*, 533, 1979.

Krall, N. A., and A. W. Trivelpiece, *Principles of Plasma Physics*, p. 473, McGraw-Hill, New York, 1973.

Krimigis, S. M., G. Haerendel, R. W. McEntire, G. Paschmann, and D. A. Bryant, The Active Magnetostpheric Particle Tracer Explorers (AMPTE) program, *Eos Trans. AGU*, *63*, 843, 1982.

Lemons, D. S., J. R. Asbridge, S. J. Bame, W. C. Feldman, S. P. Gary, and J. T. Gosling, The source of electrostaic fluctuations in the solar wind, *J. Geophys. Res.*, *84*, 2135, 1979.

Lühr, H., N. Klöcker, W. Oelschlägel, B. Häusler, and M. Acuña, The IRM magnetometer, *IEEE Trans. Geosci. Remote Sens.*, *GE-23*, 259, 1985.

Lühr, H., D. J. Southwood, N. Klöcker, M. W. Dunlop, W. A. C. Mier-Jedrzejowicz, R. P. Rijnbeek, M. Six, B. Häusler, and M. Acuña, In-site magnetic field observations of AMPTE's artificial comet, *Nature*, *320*, 708, 1986.

Mende, S., Morphology of the magnetospheric barium release, *J. Geophys. Res.*, *78*, 5751, 1973.

Paschmann, G., H. Loidl, P. Obermayer, M. Ertl, R. Laborenz, N. Sckopke, W. Baumjohann, C. W. Carlson, and D. W. Curtis, The plasma instrument on AMPTE IRM, *IEEE Trans. Geosci. Remote Sens.*, *GE-23*, 1985.

Pongratz, M. B., Large scientific releases, *Adv. Space Res.*, *1*, 253, 1981.

Rees, D., T. J. Hallinan, H. C. Stenbaek-Nielsen, M. Mendillo, and J. Baumgardner, Optical observations of the AMPTE artificial comet release from the northern hemisphere, *Nature*, *320*, 704, 1986.

Rodgers, D. J., A. J. Coates, A. D. Johnstone, M. F. Smith, D. A. Bryant, D. S. Hall, and C. P. Chaloner, UKS plasma measurements near the AMPTE artificial comet, *Nature*, *320*, 712, 1986.

Rodriguez, P., and D. A. Gurnett, Electrostatic and electromagnetic turbulence associated with the earth's bow shock, *J. Geophys. Res.*, *80*, 19, 1975.

Scarf, F. L., R. W. Fredricks, L. A. Frank, and M. Neugebauer, Nonthermal electrons and high-frequency waves in the upstream solar wind, 1, Observations, *J. Geophys. Res.*, *76*, 5162, 1971.

Scarf, F. L., F. V. Coroniti, C. F. Kennel, D. A. Gurnett, W.-H. Ip, and E. J. Smith, Plasma wave observations at Comet Giacobini-Zinner: A preliminary report, *Science*, *232*, 377, 1986.

Valenzuela, A., G. Haerendel, H. Föppl, F. Melzner, H. Neuss, E. Rigger, J. Stoecker, O. Bauer, H. Höfner, and J. Loidl, The artificial comet experiments, *Nature*, *320*, 700, 1986.

Wescott, E. M., J. D. Stolarik, and J. P. Heppner, Electric fields in the vicinity of auroral forms from motions of barium vapor releases, *J. Geophys. Res.*, *74*, 3469, 1969.

Wescott, E. M., H. C. Stenbaek-Nielsen, T. J. Hallinan, C. S. Deehr, G. J. Romick, J. V. Olson, J. G. Roederer, and R. Sydora, A high-altitude barium radial injection experiment, *Geophys. Res. Lett.*, *7*, 1037, 1980.

Winske, D., and M. M. Leroy, Diffuse ions produced by electromagnetic ion beam instabilities, *J. Geophys. Res.*, *89*, 2673, 1984.

R. R. Anderson, D. A. Gurnett, and T. Z. Ma, Department of Physics and Astronomy, University of Iowa, Iowa City, IA 52242.

O. H. Bauer, G. Haerendel, G. Paschmann, and R. A. Treumann, Max-Planck Institut für extraterrestrische Physik, 8046 Garching, Federal Republic of Germany.

R. H. Holzworth, Geophysics Program, University of Washington, Seattle, WA 98195.

H. C. Koons, The Aerospace Corporation, P. O. Box 92957, Los Angeles, CA 90009.

H. Lühr, Institut für Geophysik und Meteorologie, Technische Universität Braunschweig, 3300 Braunschweig, Federal Republic of Germany.

(Received December 3, 1985;
revised March 18, 1986;
accepted April 22, 1986.)